PAPER

Energy transfer in single phase Eu³⁺-doped Y₂WO₆ phosphors

J. Llanos,*[a] D. Espinoza[ab] and R. Castillo[a]

Inorganic phosphors based on monoclinic Y_2WO_6 doped with Eu^{3+} ions were prepared *via* conventional solid-state reactions at high temperature. A total of five samples were obtained with different Eu^{3+} concentrations (0–9%). The purity of the as-prepared phases was checked by powder X-ray diffraction (PXRD). Through the Rietveld refinement, at low concentrations Eu^{3+} ions are found to occupy preferentially the Y2 (2f) sites in the host compound. However, for higher dopant concentrations, the occupancy of the (2e) and (4g) sites becomes relevant. The excitation, emission, and time-resolved emission spectra were examined in detail. Efficient energy transfer from the $(WO_6)^{6-}$ groups to the Eu^{3+} activators was observed. The decay curves for the Eu^{3+} $^5D_0 \rightarrow {}^7F_4$ transition show a non-exponential behavior that is enhanced with increasing Eu^{3+} concentration. The experimental decay curves were fitted to the Inokuti–Hirayama model to gain some insight into the mechanism of the interaction between the Eu^{3+} ions in these phosphors.

1. Introduction

In the last decades there has been great interest in the synthesis of inorganic phosphors doped with rare-earth cations mainly because of their uses as luminescent materials in solid-state lighting devices (SSLD), plasma display panels, solar cells, optical sensors, and more recently, for applications in the new fields of nanotechnology and biotechnology.[1–6] The trivalent europium ion (Eu^{3+}) is widely used as an activator ion in many phosphors due to its characteristic red emission upon irradiation with UV light, arising from the $^5D_0 \rightarrow {}^7F_J$ ($J = 0,4$) transitions.[7–9] The $^5D_0 \rightarrow {}^7F_1$ transition is a magnetic dipole (MD) transition and, hence, its intensity is largely independent from the chemical environment of the Eu^{3+} cation in the host matrix. In contrast, the electric dipole (ED) $^5D_0 \rightarrow {}^7F_2$ transition is one of the so-called "hypersensitive transitions", which means that its appearance and intensity is greatly influenced by the local symmetry of the Eu^{3+} ion. It is well known that the asymmetric ratio (R) between the intensities of the two ED and MD transitions, $^5D_0 \rightarrow {}^7F_2/^5D_0 \rightarrow {}^7F_1$, can be used as a probe of the local symmetry of the Eu^{3+} ions in a host material.[10,11] For example, in $BaTiO_3 : Eu^{3+}$, $R > 1$ indicates that the proportion of Eu^{3+} ions in non-centrosymmetric sites is larger than that in centrosymmetric ones, which is in good agreement with the distortion of the lattice found in Eu-doped samples resulting in a change in the local symmetry from octahedral (O_h) to a non-centrosymmetric C_{4v} symmetry.[12]

Inorganic phosphors typically consist of an inert host material, normally either oxides, nitrides/oxynitrides, or sulfides/oxysulfides, doped with a small concentration of activator ions. In particular, metal oxides containing d^0 transition metal ions, such as VO_4^{3-}, MoO_4^{2-}, or WO_4^{2-} have attracted much attention as host lattices in inorganic phosphors. Tungstates with different stoichiometries, such as Y_2WO_6, have been studied less extensively, probably due to their rich crystallographic variation. Depending on the synthetic method, Y_2WO_6 can crystallize in a tetragonal (S.G. $P4/nmm$), monoclinic (S.G. $P2/c$), or orthorhombic (S.G. $P2_1ab$) form.[13–16] On the other hand, Borchardt identified Y_2WO_6 as a bright photoluminescent material that emitted a pale blue light under ultraviolet excitation[17] showing that the excited tungstate groups can effectively transfer energy to doping activator ions.

In the past few years, we have been actively involved in the preparation and characterization of new red-emitting phosphors.[18–20] In this paper, $Y_{2-x}Eu_xWO_6$ red phosphors were synthesized *via* solid-state reactions and their photoluminescent features were studied. We have carried out a detailed analysis of the energy transfer process between the luminescent excited levels of the dopant Eu^{3+} ions as a function of their concentration and the interaction between these ions and the host lattice structure. The energy transfer process is found to be well described by the Inokuti–Hirayama model.

2. Experimental

2.1. Synthesis

All $Y_{2-x}Eu_xWO_6$ samples in this study were prepared at high temperature using solid-state reactions[21] starting from

[a]*Departamento de Química, Universidad Católica del Norte, Casilla 1280, Antofagasta, Chile. E-mail: jllanos@ucn.cl; Tel: +56 55 2 355615*

[b]*Departamento de Química, Universidad de Chile, Las Palmeras 3425, Santiago, Chile*

a thoroughly ground mixture of the corresponding oxides, Y_2O_3, Eu_2O_3, and WO_3, in stoichiometric proportions. These mixtures were placed in an alumina boat and heated at 973 K for 10 h before being cooled to below 400 K. The samples were then removed from the crucible, ground into a powder, and reheated for 10 h at 1273 K. The procedure was repeated and the sample was finally heated to 1373 K for another 10 h. Optical inspection of the products showed homogeneous powders with a white color. All of the above synthetic processes were performed under an air atmosphere.

2.2. Characterization

To verify the purity of the phases, powder X-ray diffraction (PXD) data were collected using a Bruker D8 Advance diffractometer fitted with a graphite monochromator. The spectra were collected across the range $10° \leq 2\theta \leq 60°$, using Cu Kα radiation ($\lambda = 1.54057$ Å) generated at 40 kV and 30 mA. The excitation spectra were measured using a JASCO FP-6500 spectrofluorometer with a 150 W xenon lamp as the excitation source. The emission spectra were obtained by exciting the samples at 300 nm using a 400 W Oriel xenon lamp. The spectra were recorded with a system of two convex lenses that collimated and focalized the Eu^{3+} emission into an optical fiber coupled to a 0.3 m single grating spectrometer (Andor Shamrock-3031-B). The final measurement was done using a cooled CCD detector (Newton DU920 N) with a resolution of 0.7 nm and an integration time of 2 s. For the lifetime measurements, a tunable optical parameter oscillator (OPO) was used as the excitation source (10 Hz repetition rate, 8 ns pulse temporal width) and the time resolved emission was focused on the entrance slit of a monochromator (Triax 180) coupled with a photomultiplier (Hamamatsu r928). The signal was acquired and averaged by an oscilloscope (Lecroy Wavesurfer 424). All measurements were carried out at room temperature.

Thermogravimetry (TG) and differential scanning calorimetry (DSC) analyses were carried out on a STA 448 Jupiter F3 type simultaneous thermal analyzer (Netzsch). The samples used for TG and DSC were powders of about 69 mg in weight. The sample cells were aluminum oxides pans. The parent reagents were heated up to 1373 K at a heating rate of 5 K min^{-1} under flowing of nitrogen atmosphere at 20 mL min^{-1}.

3. Results and discussion

Samples for a total of five different compositions were synthesized in the $Y_{2-x}Eu_xWO_6$ system with $x \cong 0$, 0.02, 0.06, 0.14 and 0.18. The powder X-ray diffraction patterns for these compounds are similar to those for the monoclinic Y_2WO_6 phase previously reported in the ICSD (Inorganic Crystal Structure Data) database and by Efremov et al.,[22,23] indicating that all samples crystallized isostructurally adopting the monoclinic Y_2WO_6 structure belonging to the $P2/c$ space group (no. 13). In this structure there are three different crystallographic sites for the Y^{3+} ion. Two of them are eight-fold coordinated by O$^-$ atoms, whereas in the third one, the lanthanide ion is seven-fold coordinated by oxygen atoms (Fig. 1). Upon doping, the trivalent europium ions are expected to occupy the yttrium sites in Y_2WO_6 : Eu^{3+} since the ionic radii of Eu^{3+}, $r =$
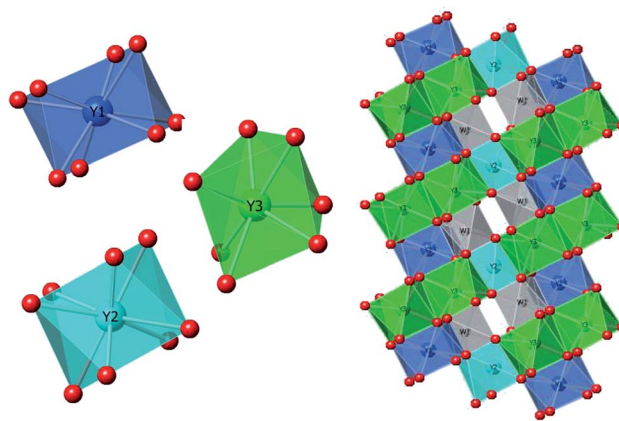

Fig. 1 Scheme of the Y_2WO_6 structure indicating three different sites for the lanthanide ions.

106.6 pm (C.N. = 8) and $r = 101.0$ pm (C.N. = 7), are only slightly larger than those of Y^{3+}, $r = 96$ pm (C.N. = 8) and 101.9 pm (C.N. = 7).[24] The values of the cell parameters, confirmed by a Le Bail refinement,[25,26] for all compounds are given in Table 1, together with their standard deviations. The variation of the unit cell with the Eu^{3+} content confirms the existence of a range of solid solutions represented by the formula $Y_{2-x}Eu_xWO_6$ ($x \cong 0.02$, 0.06, 0.14 and 0.18).

Rietveld refinements for the $Y_{2-x}Eu_xWO_6$ ($x \cong 0.0$, 0.02, 0.18) structures were carried out using the Jana 2006 software.[27] The calculated patterns are consistent with the experimental data (see Fig. 2). The occupation factors, refinement parameters and refined compositions are shown in Table 2. As seen, the crystallographic volume of the samples increases with increasing Eu^{3+} content, while the lattice parameters change only slightly.

Changes in the cell parameters are correlated with the occupation of the Eu^{3+} ions in the Y^{3+} positions. One can see that at low concentrations Eu^{3+} ions occupy preferentially the Y2 (2f) sites, while the occupancy of the Y1 (2e) and Y3 (4g) sites becomes relevant as the concentration of Eu^{3+} ions increases. This trend in the occupancy of the different sites explains some of the irregularities in the variation of the unit cell parameters for the doped phases (vide supra). On the other hand, the refined compositions obtained through the Rietveld refinement are in good agreement with the TG-DSC experiments (Fig. 3) ruling out the possibility of volatilization of WO_3 during the synthesis process.

The emission spectrum of un-doped Y_2WO_6 under 300 nm UV radiation is shown in Fig. 4. As it has been previously described, tungstate based materials emit blue light (450 nm) themselves under ultraviolet radiation.[28] The excitation spectrum of the 450 nm emission for the un-doped sample is dominated by a broad band that can be attributed to the absorption by $(WO_6)^{6-}$ groups with a peak centered at about 300 nm (Fig. 4). The decay curve of the blue emission under pulsed laser excitation (300 nm) shown in the inset of Fig. 4 is non-exponential with an intrinsic lifetime of $\tau = 6.65$ μs.

PLE spectra of the Eu-doped samples are similar to those previously reported.[15] They exhibit a broad band centered at

Table 1 Cell parameters for Eu^{3+} doped Y_2WO_6 samples. Standard deviations are given in parentheses

Compound	a (Å)	b (Å)	c (Å)	β (°)	Vol. (Å)^3	Ref.
Y_2WO_6	7.578(9)	5.330(8)	11.361(18)	104.36(9)	444.6(12)	22 and 23
$Y_{1.98}Eu_{0.02}WO_6$	7.578(14)	5.331(10)	11.364(2)	104.36(11)	444.8(14)	
$Y_{1.94}Eu_{0.06}WO_6$	7.578(8)	5.331(10)	11.365(1)	104.33(6)	444.8(12)	
$Y_{1.90}Eu_{0.10}WO_6$	7.579(1)	5.333(7)	11.367(1)	104.32(7)	445.2(12)	
$Y_{1.86}Eu_{0.14}WO_6$	7.578(1)	5.333(7)	11.368(2)	104.31(1)	445.2(14)	
$Y_{1.82}Eu_{0.18}WO_6$	7.581(15)	5.335(10)	11.372(2)	104.32(12)	445.7(16)	
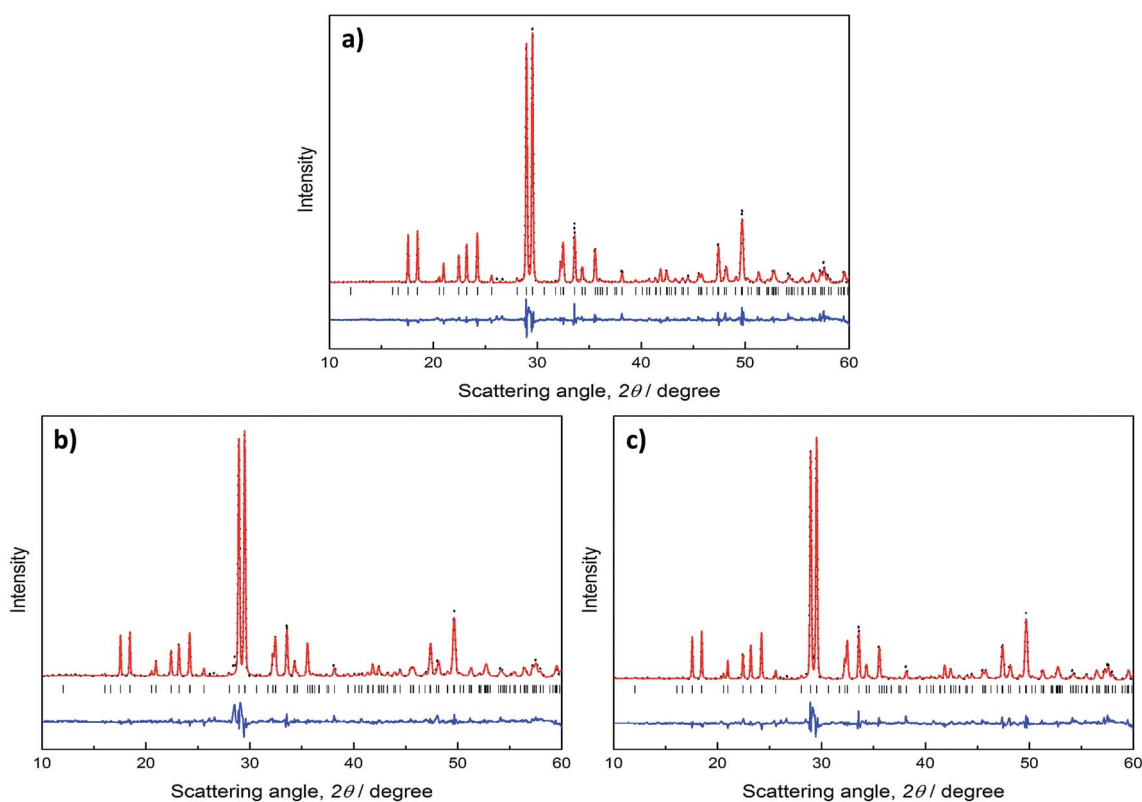
Fig. 2 Rietveld refinement results for (a) Y_2WO_6; (b) $Y_{1.98}Eu_{0.02}WO_6$ and (c) $Y_{1.82}Eu_{0.18}WO_6$. The blue line shows the difference between observed and calculated data.

about 300 nm along with very weak f–f transitions at about 395 nm ($^7F_0 \rightarrow ^5L_6$), 465 nm ($^7F_0 \rightarrow ^5D_2$), and 540 nm ($^7F_0 \rightarrow ^5D_1$). The broad, intense band consists of overlapping O^{2-}–Eu^{3+} and O^{2-}–W^{6+} charge transfer bands.

Room temperature emission spectra of the $Y_{2-x}Eu_xWO_6$ ($x =$ 0.0, 0.02, 0.06, 0.14, and 0.18) samples are shown in Fig. 5. The intra-configurational 4f–4f transitions of the Eu^{3+} ions originating from the $^5D_0 \rightarrow ^7Fj$ ($J = 0$–4) transitions were identified. The most intense emission corresponds to the electric dipole $^5D_0 \rightarrow ^7F_2$ transition centered at approximately 610 nm. The emission spectra are also characterized by the band at about 450 nm, originating from the $(WO_6)^{6-}$ groups of the host matrix. This emission band disappears when the concentration of the dopant ion is increased. The variation of the emission intensity at 450 nm with the dopant concentration is shown in the inset of Fig. 6. It is observed that while the intensity of the band at 450 nm decreases, that of the band at 610 nm increases for concentrations up to $x = 0.14$. This phenomenon implies that an energy transfer from the $(WO_6)^{6-}$ groups to the Eu^{3+} ions must occur. At the same time, we observe that the PL intensity decreases when x exceeds 0.14 due to concentration quenching, related to an energy transfer between activator centers. For a good characterization of the PL behavior in this system it is therefore necessary to determinate the critical distance between donors (activator) and acceptors (quenching site) that can be estimated using the equation proposed by Blasse *et al.*:[29]

$$R_0 = 2\left(\frac{3V}{4\pi\chi_c N}\right)^{1/3} \quad (1)$$

where $R_0 =$ critical distance, $V =$ the unit cell volume, $\chi_c =$ the critical concentration, and $N =$ the number of formula units in the unit cell. Using $V = 445.2$ Å^3, $\chi_c = 0.14$, and $N = 4$, the critical distance is found to be $R_0 = 11.5$ Å.

Table 2 Cell parameters, occupation factors, refined parameters and refined compositions for $Y_{2-x}Eu_xWO_6$ ($x \cong$ 0.0, 0.02, 0.18). Atomic positions are referenced in ref. 22 and 23

Compound	Y_2WO_6	$Eu_{0.02}Y_{1.98}WO_6$	$Eu_{0.18}Y_{1.82}WO_6$
$a/\text{Å}$	7.578(12)	7.578(14)	7.581(15)
$b/\text{Å}$	5.330(8)	5.331(10)	5.335(10)
$c/\text{Å}$	11.361(18)	11.364(2)	11.372(2)
$\beta/(°)$	104.36(9)	104.36(11)	104.32(12)
$V/\text{Å}^3$	444.6(12)	444.8(14)	445.7(16)
Site occupancy			
Y1/Eu1 (2e)	1.00(4)	1.00(3)/0.00(3)	0.83(7)/0.17(7)
Y2/Eu2 (2f)	1.00(5)	0.95(7)/0.05(7)	0.86(7)/0.14(7)
Y3/Eu3 (4g)	1.00(3)	0.98(5)/0.02(5)	0.90(5)/0.10(5)
$R_p/(\%)$	13.51	13.87	12.77
$R_{wp}/(\%)$	20.41	20.89	20.13
$R_F/(\%)$	5.89	7.03	6.57
Refined composition	$Y_{2.00(5)}WO_6$	$Eu_{0.04(3)}Y_{1.96(3)}WO_6$	$Eu_{0.25(9)}Y_{1.75(9)}WO_6$

In order to evaluate the efficiency of the energy transfer (η_{ET}) from the host matrix to the Eu^{3+} ions, we estimated the emission intensities of the matrix in the presence (I_s) and absence (I_{s_0}) of the activator ion, using these values to calculate η_{ET} using the following expression:[30–32]

$$\eta_{ET} = 1 - \frac{I_s}{I_{s_0}} \qquad (2)$$

The quantum efficiency of the activator ions (QE) $\eta_{Eu^{3+}}$ can be calculated using the relevant emission spectra and the following expression:

$$\eta_{Eu^{3+}} = \frac{\int_{hv}^{I_{Eu^{3+}}} d\lambda}{\int_{hv}^{I_{s_0}-I_s} d\lambda} = \frac{\int I_{Eu^{3+}} d\lambda}{\int \lambda (I_{s_0} - I_s) d\lambda} \qquad (3)$$

where $I_{Eu^{3+}}$ is the emission of the Eu^{3+} ion, and the remaining symbols have their usual meaning described in eqn (2) (*vide supra*). The calculated η_{ET} and $\eta_{Eu^{3+}}$ values are shown in Table 3, where it is observed that the η_{ET} values increase along with the increase in the Eu^{3+} concentration, while the values of $\eta_{Eu^{3+}}$ reach a maximum when $x = 0.14$.

These results are in good agreement with those reported by Z. Zhao *et al.* where the optimal concentration of Eu^{3+} in the Y_2WO_6 matrix is found to be $x = 0.13$ (ref. 33) and with those reported by Li. *et al.*, where $x = 0.09$.[16] The behavior found for the Y_2WO_6 matrix is quite different from that found for the $KLa(WO_4)_2$ matrix, for example, where the critical concentration is reached when the Eu^{3+} concentration is about 40% at.[34]

As shown in Fig. 6, room temperature emission decay curves upon excitation at 300 nm were measured for the Eu^{3+} doped samples with different concentrations of the rare-earth ion. Our studies are focused mainly in the $^5D_0 \rightarrow {}^7F_4$ transition, because the broad emission band of the matrix overlaps the emission corresponding to the $^5D_0 \rightarrow {}^7F_2$ transition at 610 nm. The decay curves for the Eu^{3+} $^5D_0 \rightarrow {}^7F_4$ transition emission show a non-exponential behavior that is enhanced with increasing Eu^{3+} concentration. The non-exponential character of the decay curves can be explained by taking into account the fact that at intermediate doping concentrations the Eu^{3+} and the Y^{3+} ions are randomly distributed in the Y^{3+} sites in Y_2WO_6.[35] According to Collins *et al.*[36] there are three different regimes of donor decay: (i) no diffusion, where the energy transfer occurs between
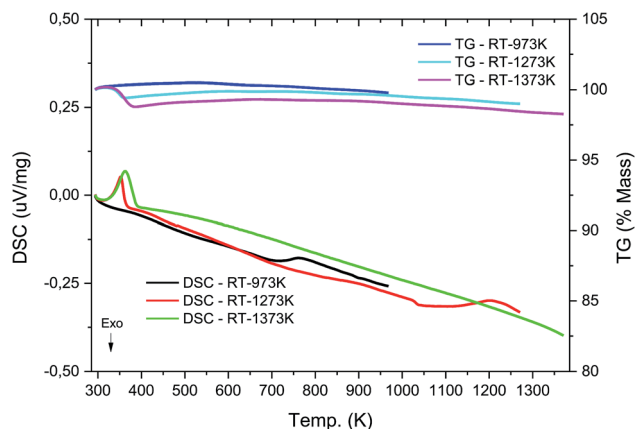

Fig. 3 TG-DSC analysis of the heating cycles in the synthesis process of the doped samples.
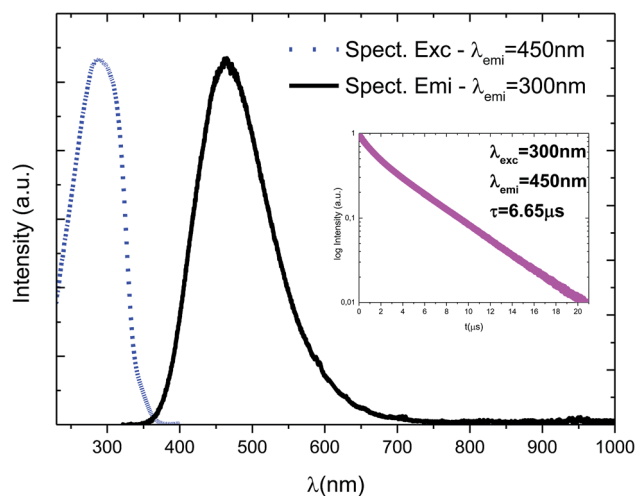

Fig. 4 Emission ($\lambda_{ex} = 300$ nm) and excitation spectra ($\lambda_{em} = 450$ nm) of Y_2WO_6. The inset shows the decay curve of the emission band of the un-doped host structure.
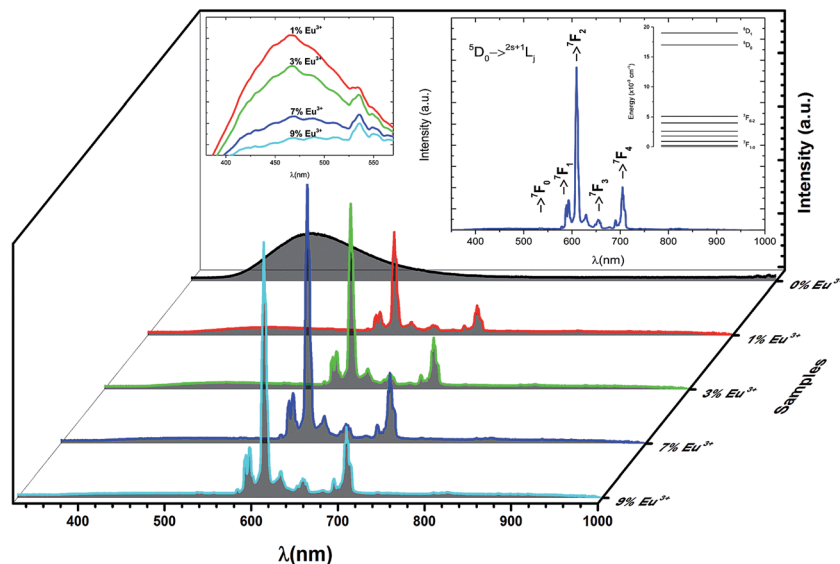
Fig. 5 Emission spectra of $Y_{2-x}Eu_xWO_6$ ($x \cong 0$, 0.02, 0.06, 0.14 and 0.18) (λ_{ex} = 300 nm). The inset shows that the emission band at 450 nm disappears along with the Eu^{3+} concentration, the emission spectrum of $Y_{1.86}Eu_{0.14}WO_6$ and a partial energy level diagram of Eu^{3+} ions.

donor and acceptor with little or no diffusion among donors; (ii) diffusion limited decay, where there is significant diffusion among donors before donor–acceptor energy transfer occurs; and (iii) fast diffusion, during which the diffusion among donors is so fast that the excited atom rapidly comes close enough to an acceptor to allow for a donor–acceptor energy transfer. The non-exponential behavior of the decay curves reveals that the energy transfer process occurs with little or no

Fig. 6 Eu^{3+} concentration dependence of decay curves of $Y_{2-x}Eu_x$-WO_6 (λ_{ex} = 300 nm, λ_{em} = 704 nm).

Table 3 Energy transfer efficiency and quantum efficiency (Eu^{3+}) of the synthetized phosphors

Compound	η_{ET} (%)	$\eta_{Eu^{3+}}$ (%)
$Y_{1.98}Eu_{0.02}WO_6$	89.3	27.7
$Y_{1.94}Eu_{0.06}WO_6$	91.1	47.5
$Y_{1.86}Eu_{0.14}WO_6$	94.8	63.1
$Y_{1.82}Eu_{0.18}WO_6$	96.6	61.2

diffusion among the donors. Hence we use the Inokuti–Hirayama model in order to analyze the decay curves.[37] In this model, it is assumed that the activator ions are randomly distributed in the host structure. The Inokuti–Hirayama equation can be formulated as follows:

$$I_t = I_0 \ \exp\left[-\left(\frac{t}{\tau}\right) - \left(\frac{C}{C_0}\right) \Gamma\left(1 - \frac{3}{s}\right)\left(\frac{t}{\tau}\right)^{3/s} \right] \quad (4)$$

where τ is the intrinsic lifetime of a single ion (0.85 ms in our case, obtained from the sample with the lowest Eu^{3+} concentration), C is the acceptor concentration, C_0 the critical concentration of acceptors, $\Gamma\left(1 - 3/s\right)$ the gamma function, and s a parameter that depends on the type of interaction (for dipole–dipole interactions $s = 6$). The critical concentration C_0 is defined as: $C_0 = 3/(4\pi R_0^3)$, where R_0 is the critical transfer distance, which is defined as the distance between donor and acceptor at which the probability of energy transfer per unit time is equal to the probability of decay of the donor per unit time. Assuming a dipole–dipole character for the interaction between donor and acceptor ions, the energy transfer parameter (Q) is given by:

$$Q = \frac{4\pi}{3}\Gamma\left(1 - \frac{3}{s}\right)C(R_0)^3 \quad (5)$$

where for a dipole–dipole interaction $\Gamma\left(1 - \frac{3}{s}\right) = \Gamma\left(\frac{1}{2}\right) = \sqrt{\pi} = 1.77$. The energy transfer parameter (Q) can also be described as follows:

$$Q = \frac{4\pi}{3}\Gamma\left(1 - \frac{3}{s}\right)C(C_{DA}\tau)^{3/s} \quad (6)$$

where C_{DA} is the donor–acceptor energy transfer parameter. By combining eqn (5) and (6), C_{DA} can be defined as:
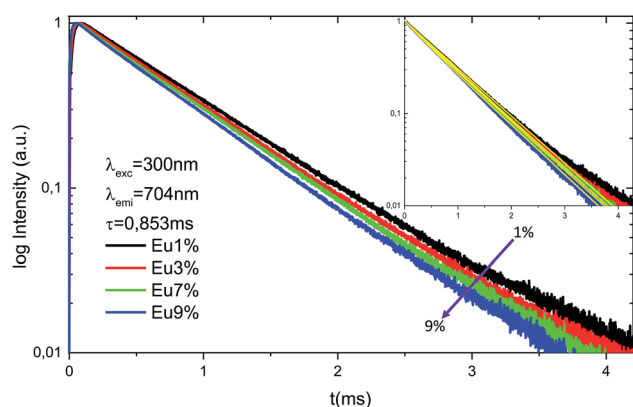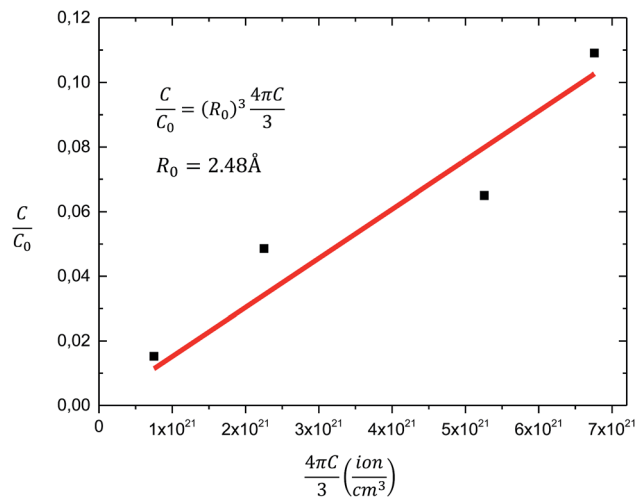
Fig. 7 Plot of C/C_0 vs. $(4\pi C/3)$. The C/C_0 values are taken from the fitting results of dipolar interaction.

$$C_{DA} = \frac{(R_0)^6}{\tau}. \tag{7}$$

The unit 'number of ions per cm^3' is used to describe the concentration of both donor and acceptors ions and the intrinsic lifetime of a single ion, $\tau = 0.85$ ms, was obtained from the sample with the lowest concentration of Eu^{3+} (*vide supra*). By replacing $(R_0)^3$ in eqn (5) by the expression $R_0^3 = 3/(4\pi c_0)$ and rearranging the equation, we get the following expression:

$$\frac{C}{C_0} = R_0^3 \frac{4\pi C}{3} \tag{8}$$

from which we can estimate R_0, the critical distance, determining the slope of the C/C_0 vs. $(4\pi C)/3$ plot by a simple linear fitting. The data points and the fitted line are shown in Fig. 7 from where $R_0 = 2.48$ Å and $C_0 = 1.57 \times 10^{22}$ ions per cm^3. The value of R_0 is of the same order of magnitude as, but not comparable to, that obtained from Blasse's equation (11.5 Å). The same deviation has been observed for other RE-doped host structures and the discrepancy could originate from the assumption that C (quenching site concentration) is equal to the Eu^{3+} concentration.[38,39] As can be observed in Fig. 5, the temporal evolution of decays obtained for different Eu^{3+} concentrations were fitted according to the Inokuti–Hirayama model. Based on these fits, the donor–acceptor energy transfer parameter (C_{DA}) was calculated using eqn (5). A value of $C_{DA} = 2.73 \times 10^{-43}$ cm^6 s^{-1} was obtained, which is similar to that obtained for other matrices.[38]

4. Conclusions

We prepared Y_2WO_6 based phosphors doped with different concentrations of Eu^{3+} *via* a classic solid-state reaction at high temperature. The luminescent properties of the resultant compounds were investigated. The excitation spectrum is dominated by a broad band consisting of the overlapping O^{2-}–Eu^{3+} and O^{2-}–WO_6^{6+} charge transfer bands, as well as three bands corresponding to the excitations of electrons from the Eu^{3+} ground state to different excited 4f levels. The emission spectra have a characteristic peak caused by the electric dipole $^5D_0 \rightarrow {}^7F_2$ transition centered at 610 nm. An emission band centered at about 450 nm originating from the $(WO_6)^{6-}$ groups of the host structure is also observed. Moreover, it is found that while the intensity of the band at 450 nm decreases, that of the band at 610 nm increases for dopant concentrations up to $x = 0.14$ implying the presence of an energy transfer from the host to the Eu^{3+} ions.

The measured decay curves are quite well described by the Inokuti–Hirayama model assuming a dipole–dipole interaction. All results indicate that Eu^{3+} ions are localized randomly in the structure ruling out the possibility of cluster formation.

References

1 T. Jüstel, H. Nikols and C. Ronda, *Angew. Chem., Int. Ed.*, 1998, **37**, 3084.
2 J. T. Ingle, R. P. Sonekar, S. K. Omanwar, Y. Wang and L. Zhao, *J. Alloys Compd.*, 2014, **608**, 235.
3 H. Höppe, *Angew. Chem., Int. Ed.*, 2009, **48**, 3572.
4 J.-C. Bünzli, *Chem. Rev.*, 2010, **110**, 2729.
5 D. Jaque and F. Vetrone, *Nanoscale*, 2012, **4**, 4301.
6 L. Zhou, J. Huang, F. Gong, Y. Lan, Z. Tong and J. Sun, *J. Alloys Compd.*, 2010, **495**, 268.
7 J. Llanos, R. Castillo, D. Espinoza, R. Olivares and I. Brito, *J. Alloys Compd.*, 2011, **509**, 5295.
8 F. Meng, H. Zhang, C. Chen, S. I. Kim and H. J. Seo, *J. Alloys Compd.*, 2016, **671**, 150.
9 H. Marzougui, I. R. Martín, S. Attia-Essaies, D. B. Hassen-Chehimi, E. Lalla and S. B. F. León-Luis, *Opt. Mater.*, 2015, **46**, 339.
10 U. Rambabu and S.-D. Han, *RSC Adv.*, 2013, **3**, 1368.
11 G. Gao and L. Wondraczek, *Opt. Mater. Express*, 2014, **4**, 480.
12 S. Fuentes, N. Barraza, E. Veloso, R. Villarroel and J. Llanos, *J. Alloys Compd.*, 2013, **569**, 52.
13 J. Huang, J. Xu, H. Li, H. Luo, X. Yu and Y. Li, *J. Solid State Chem.*, 2011, **184**, 843.
14 R. Hao, Q. Meng, W. Liu and H. Liu, *J. Rare Earths*, 2013, **31**, 864.
15 J. Llanos, D. Olivares, V. Manríquez, D. Espinoza and I. Brito, *J. Alloys Compd.*, 2015, **628**, 352.
16 X. Shi, J.-G. Li, Q. Zhu, X. Li and X. Sun, *J. Alloys Compd.*, 2017, **695**, 1984.
17 H. J. Borchardt, *J. Chem. Phys.*, 1963, **2**, 170.
18 J. Llanos and R. Castillo, *J. Lumin.*, 2009, **129**, 465.
19 J. Llanos and R. Castillo, *J. Lumin.*, 2010, **130**, 1124.
20 J. Llanos, R. Castillo, I. R. Martin, L. L. Martin, P. Haro-González and J. González-Platas, *J. Lumin.*, 2014, **145**, 553.

21 Z. Zhang, W. Wang, M. Shang and W. Yin, *J. Hazard. Mater.*, 2010, **177**, 1013.

22 V. A. Efremov, A. V. Tyulin, V. K. Trunov, O. V. Kudin, V. K. Yanosvskii and V. I. Voronkoba, *Kristallografiya*, 1984, **29**, 904.

23 Inorganic Crystal Structure Database, ICSD, Fachinformationzentrum Karlsruhe, Release 1/2016, Coll. Code. #20955.

24 R. D. Shannon, *Acta Crystallogr., Sect. A: Cryst. Phys., Diffr., Theor. Gen. Crystallogr.*, 1976, **32**, 751.

25 A. L. Bail, *Powder Diffr.*, 2005, **20**, 316.

26 A. L. Bail, H. Duroy and J. L. Fourquet, *Mater. Res. Bull.*, 1988, **23**, 447.

27 V. Petricek, M. Dusek and L. Palatinus, *J. Crystallogr.*, 2014, **229**, 345.

28 X.-Y. Chen, Z.-J. Zhang, L.-L. Zhu, M. Xu, H. Wang, A.-G. Li and J.-T. Zhao, *Appl. Surf. Sci.*, 2014, **317**, 730.

29 G. Blasse, *Philips Res. Rep.*, 1969, **24**, 131.

30 U. Caldiño, J. Hernández-Pozos, C. Flores, A. Speghini and M. Bettinelli, *J. Phys.: Condens. Matter*, 2005, **17**, 7297.

31 U. Caldiño, A. Speghini and M. Bettinelli, *J. Phys.: Condens. Matter*, 2006, **18**, 3499.

32 G. Ju, Y. Hu, L. Chen, X. Wang, Z. Mu, H. Wu and F. Kang, *J. Lumin.*, 2012, **132**, 1853.

33 J. Li, Z. Wu, X. Sun, X. Zhang, R. Dai, J. Zuo and Z. Zhao, *J. Mater. Sci.*, 2017, **52**, 3110.

34 M. Kavi Rasu, D. Balaji and S. Moorthy Babu, *J. Lumin.*, 2015, **170**, 547.

35 P. Vergeer, T. J. H. Vlugt, M. H. F. Kox, M. I. den Hertog, J. P. J. M. van der Erden and A. Meijerink, *Phys. Rev. B: Condens. Matter Mater. Phys.*, 2005, **71**, 014119.

36 J. Collins, M. Geen, M. Bettinelli and B. Di Bartolo, *J. Lumin.*, 2012, **132**, 2626.

37 M. Inokuti and F. Hirayama, *J. Chem. Phys.*, 1965, **43**, 1978.

38 X. Zhang, Z. Zhang, S. I. Kim, Y. M. Yu and H. J. Seo, *Ceram. Int.*, 2014, **40**, 2173.

39 K.-S. Sohn, Y. G. Choi, Y. Y. Choi and H. D. Park, *J. Electrochem. Soc.*, 2000, **147**, 3552.